J. Fluid Mech. (2002), *vol.* 457, *pp.* 285–294.
DOI: 10.1017/S0022112002007760 Printed in the United Kingdom

Active electrostatic stabilization of liquid bridges in low gravity

By DAVID B. THIESSEN, MARK J. MARR-LYON AND PHILIP L. MARSTON

Department of Physics, Washington State University, Pullman, WA 99164-2814, USA

(Received 10 November 2001 and in revised form 28 December 2001)

In experiments performed aboard NASA's low-gravity KC-135 aircraft, it was found that rapid active control of radial electrostatic stresses can be used to suppress the growth of the (2,0) mode on capillary bridges in air. This mode naturally becomes unstable on a cylindrical bridge when the length exceeds the Rayleigh–Plateau (RP) limit. Capillary bridges having a small amount of electrical conductivity were deployed with a ring electrode concentric with each end of the bridge. A signal produced by optically sensing the shape of the bridge was used to control the electrode potentials so as to counteract the growth of the (2,0) mode. Occasionally the uncontrolled growth of the (3,0) mode was observed when the length far exceeded the RP limit. Rapid breakup from the growth of the (2,0) mode on long bridges was confirmed following deactivation of the control.

1. Introduction

The Rayleigh–Plateau (RP) instability of a liquid cylinder in the absence of gravity normally prevents the formation of cylindrical liquid bridges which have a length greater than their circumference. The fundamental significance of this instability is widely recognized (Powers *et al.* 1998). The instability involves the growth of the (2,0) mode which is an axisymmetric varicose deformation of one wavelength in the axial direction. Thus one half of the cylinder swells while the other half thins until the bridge pinches into two unequal parts plus one or more satellite drops. The stability of a liquid bridge with cylindrical volume depends only on the slenderness, S, which is the ratio of the length to diameter of the bridge. The RP stability limit thus occurs for a slenderness of $S_{\max} = L_{\max}/D = 2\pi R/D = \pi$. Methods for stabilizing liquid bridges beyond the RP limit include both passive and active control methods. In passive methods, axial non-uniformity in the bridge diameter is automatically countered by the nature of the stabilizing field. Passive control methods include the use of static axial electric fields to stabilize dielectric bridges (Sankaran & Saville 1993; Ramos, González & Castellanos 1994; Burcham & Saville 2000) and a high-intensity ultrasonic standing wave of the appropriate wavelength applied in a lateral direction with the bridge positioned at a pressure node of the standing wave (Marr-Lyon, Thiessen & Marston 2001). Active control methods based on the rapid control of applied stresses have so far only been applied to stabilizing the bridge against the growth of the (2,0) mode. This allows extending the bridge beyond the RP limit; however, at a slenderness of 4.49 … the (3,0) mode (one and a half wavelengths) becomes unstable.

Rapid active control methods involve sensing the amplitude of the (2,0) mode and applying a mode-coupled feedback stress to counter the growth of the mode. Acoustic radiation pressure (Marr-Lyon, Thiessen & Marston 1997), and electrostatic stresses (Marr-Lyon *et al.* 2000) have been successfully used with feedback schemes to actively stabilize bridges beyond the RP limit. The active stabilization of electrically conducting liquid bridges using feedback control of radial electrostatic stresses has been previously demonstrated in a Plateau tank (Marr-Lyon *et al.* 2000). That publication indicates that the required amount of electrical conductivity is far less than for stabilization based on induced eddy currents (Castellanos & González 1994). In this work the active electrostatic method is extended to conducting bridges in air in the low-gravity environment of a NASA KC-135 aircraft flying parabolic manoeuvres. Stabilization of liquid bridges in air using a feedback scheme is more challenging than for the case in a Plateau tank because of the reduction in damping and inertia associated with the surrounding fluid. A further complication of the KC-135 environment is aircraft vibration. For this reason our experiments were performed in a free-float experimental package released from contact with the aircraft for periods of up to 10 s during a parabolic manoeuvre.

The active control method considered here differs in several ways from an approach to the stabilization of liquid columns based on the control of axial flow in an outer liquid bath (Lowry & Steen 1997; Chen *et al.* 1999). In the approach described by those authors an internal connecting rod is placed along the axis of the liquid bridge. The Bond number is positive so that the bridge sags in the absence of flow and an upward axial flow is driven in the outer liquid. The flow rate may be controlled to establish a stable but non-cylindrical profile, provided the column is not too long. For comparison, the generic active control strategy considered here may be used even if the Bond number vanishes, though there are significant requirements on the bandwidth of the control system (Marr-Lyon *et al.* 1997). The radial control stresses must be applied rapidly so as to stiffen the (2,0) mode of the bridge without bringing about a negative damping rate. It appears to be at least plausible that rapid active control methods could be applied to the (3,0), or other higher-order modes, with a more sophisticated optical sensor and the ability to control higher-order projections of the radial stress. The control strategy considered here is also different from a technique which has been demonstrated for temporal adjustment of the effective Bond number of a bridge of paramagnetic liquid in air based on the modulation of an inhomogeneous magnetic field (Mahajan *et al.* 2000).

Varicose instabilities on liquid columns in air (or in other gases) are relevant to a variety of situations. The control method described here, or generalizations of it based on more sophisticated optical sensors and arrays of electrodes, could make it possible to affect the growth of one or more modes on liquid columns. Examples of situations where rapid active control of radial stresses may be beneficial include drop formation from liquid jets (Lin & Reitz 1998) and the extension of the length of molten nearly cylindrical float zones. The reason for extending the length of float zones (made possible by the suppression of the RP instability) is the reduction of thermal gradients in the solid as well as in the liquid. For some materials thermal gradients in the solid place significant restrictions on the size of crystals that may be grown by float-zone methods (Cockayne 1968; Rao & Shyy 1997). Thermocapillary instabilities also place restrictions on the applications of float zones in reduced gravity (Velten, Schwabe & Scharmann 1991; Sumner *et al.* 2001; Schatz & Neitzel 2001). The thermocapillary response of liquid jets can be used to reduce the varicose growth rate (Nahas & Panton 1990).

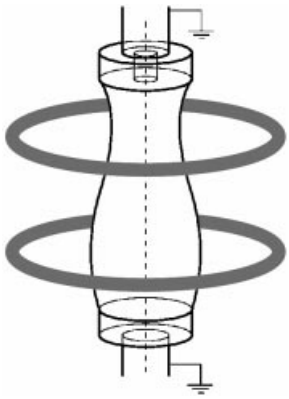

FIGURE 1. Schematic diagram of a capillary bridge with concentric ring electrodes of optimal diameter and spacing to couple into the (2,0) mode of the bridge.

2. Review of active electrostatic stabilization

The active electrostatic stabilization (AES) of liquid bridges that was reported for conducting bridges in a density-matched insulating bath (Marr-Lyon *et al.* 2000) utilized two ring electrodes which were concentric with the grounded bridge to apply the feedback stress for stabilization (figure 1). The ring diameter and spacing were chosen so that when a voltage was applied to one or other of the electrodes, the resulting stress distribution would couple optimally into the (2,0) mode of the bridge. The method involves an optical mode-sensing system that provides an error signal, V_e, proportional to the (2,0) mode amplitude, feedback circuitry that applies gain and offset to the error voltage which is then input to a high-voltage amplifier and, finally, high-voltage circuitry applies the voltages to the appropriate electrodes. The basic principle is to sense which side of the bridge is becoming thin and then apply a higher voltage to the ring electrode on that side in order to pull outward on the surface to prevent pinchoff. Three feedback algorithms identified as simple feedback, square-root feedback, and bias-potential feedback were evaluated in the Plateau-tank experiments (Marr-Lyon *et al.* 2000). In simple feedback, a voltage which is proportional to the (2,0) mode amplitude is applied to the electrode on the side of the bridge which is thinner. The problem with this method is that the Maxwell stress at the surface is proportional to the square of the voltage applied to the electrode. Thus the feedback force is not linear in the error signal, leading to non-cylindrical equilibrium shapes for the stabilized bridge. This problem is avoided if the voltage applied to the electrode is proportional to the square-root of the error voltage magnitude. Another way to make the modal projection of the feedback stress linear in the error signal is to apply bias voltages to the electrodes. If we assume that a bridge which is bulged at the bottom gives a positive error voltage, then the voltages applied to the electrodes are as follows for the three methods discussed: for simple feedback

$$V_T = KV_e, \qquad V_B = 0 \quad (V_e \geqslant 0),$$

$$V_T = 0, \qquad V_B = KV_e \quad (V_e < 0),$$

for square-root feedback

$$V_T = K|V_e|^{1/2}, \qquad V_B = 0 \quad (V_e \geqslant 0),$$

$$V_T = 0, \qquad V_B = -K|V_e|^{1/2} \quad (V_e < 0),$$

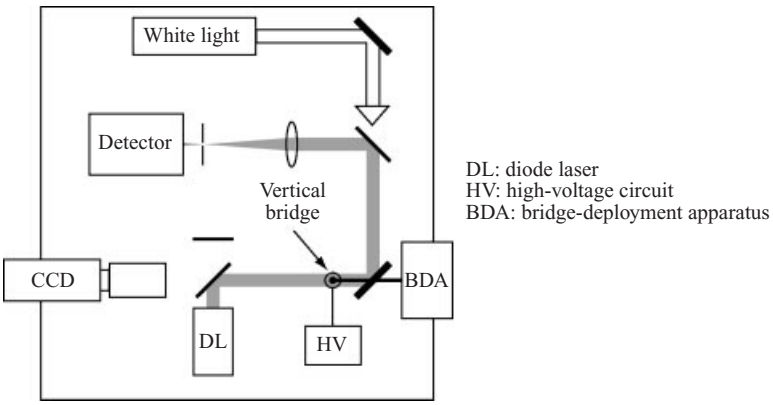

FIGURE 2. Schematic of the compact layout for the optical system used for detection of the (2,0) mode amplitude and for simultaneous imaging of the bridge. This setup resides on an optical breadboard mounted in the free-float rack.

and for bias-potential feedback

$$V_T = V_b + K V_e, \qquad V_B = -V_b + K V_e \quad \text{(for all } V_e\text{)},$$

where V_T and V_B are the voltages applied to the top and bottom electrodes respectively, K is a positive gain constant which includes the gain of the high-voltage amplifier, and V_b is a bias potential. Note that the error voltage V_e may include some offset from the signal generated by the optical detection system. This offset can be applied by the operator to correct for any asymmetries which may arise in the optical system. The simple feedback method was only infrequently tested on the KC-135 and is not emphasized here.

3. Experimental apparatus and procedure

Liquid bridges were deployed between stainless steel tips of 0.432 cm diameter. The liquids used were mixtures of glycerol, water and sodium chloride. Concentric ring electrodes of 1.23 cm diameter made of 0.12 cm diameter copper wire were used. The bridge deployment apparatus uses separate stepper motors to drive the bridge extension and liquid injection. It was difficult to produce bridges with exactly the cylindrical volume of $\pi R^2 L$ in the KC-135 environment. Bridge volumes were measured post flight by digital image analysis from images captured from video and were typically a few percent different from the cylindrical volume. A few percent difference in volume from the cylindrical value does not change the natural stability limit significantly when compared to the lengths of bridges stabilized in this work.

The major components of the experimental apparatus are the bridge deployment apparatus, the stabilization system, the imaging system, and a computer for data acquisition and experiment control. The experimental components used here are like those used in the Plateau-tank experiments described by Marr-Lyon *et al.* (2000). To avoid the effect of aircraft vibration on the experiment, the bridges are formed within an instrument rack which is released from contact with the aircraft during parabolic manoeuvres. Some experiment components reside on the free-float rack while many of the electrical components are contained within a rack which is fixed to the aircraft floor. Within the free-float rack, the optics, high-voltage circuit, electrodes, and bridge deployment system are all mounted in a compact way on an 18×18 inch

optical breadboard as shown schematically in figure 2. The operator controls the experiment from the fixed rack. An umbilical electrical cable connects the free-float rack to the fixed rack. The fixed rack contains a video monitor which can be seen by the two personnel handling the free-float rack. This allows the handlers to release the experiment at the appropriate time during the parabola. A parabola typically consists of a period of around 20 s of low gravity; however the first five seconds of this period are often of poor quality as adjustments are made to the aircraft trajectory. At the start of the low-gravity period the free-float handlers centre the rack laterally within the aircraft. The experiment operator waits until the effective gravity level is fairly low (by feel) and then deploys a bridge to a naturally stable slenderness between 2 and 3. For a bridge-stabilization experiment, the electric field is then activated and the bridge slenderness is increased to a target value beyond the RP limit. The free-float handlers try to release the rack when they see the bridge being extended beyond the initial stable slenderness and, if the bridge is being successfully stabilized, they try to allow the rack to float as long as possible. Often the parabola is not of sufficient quality to allow for full release of the rack. For bridges which are successfully stabilized, the bridge typically breaks when the rack bumps into the side of the aircraft.

The bandwidth of the control system is limited by the frequency response of the high-voltage amplifier that controls the electrode voltages. Information from the vendor (Trek Inc., Medina, N.Y.) indicates that the response is d.c. to 5 kHz with the response falling by 3 dB at 5 kHz. It is possible to estimate the effective delay in the application of the feedback stress. For low-frequency sinusoidal oscillations of frequency f (in Hz), a delay of τ for an amplifier is associated with a complex frequency response proportional to $\exp(-\mathrm{i}2\pi f\tau)$ which represents a phase delay when τ is positive. This relationship between the frequency response and τ may be modelled at low frequencies as a resistor-capacitor low-pass filter. Let $f_{3\mathrm{dB}}$ denote the 3 dB roll-off frequency response for the low-pass filter. From elementary circuit theory, if $f \ll f_{3\mathrm{dB}}$, then the response of such a filter is approximately $\exp(-\mathrm{i}f/f_{3\mathrm{dB}})$ so that $\tau \approx 1/(2\pi f_{3\mathrm{dB}})$. Taking $f_{3\mathrm{dB}} \approx 5\,\mathrm{kHz}$ gives $\tau \approx 0.03\,\mathrm{ms}$. When the square-root feedback algorithm is used, the actual delay time for the stress may differ from this value since the stress projection is proportional to the square of the amplified voltage. It is assumed in this estimate that the electrical conductance of the bridge is sufficient to maintain the potential below each electrode at ground potential within an electrical relaxation time that is shorter than τ (Marr-Lyon *et al.* 2000). An amount of sodium chloride, NaCl, was added to the bridge liquid which was more than sufficient to meet this requirement on the conductivity.

There are important differences between the damping of (2,0) mode oscillations for bridges in Plateau tanks and the damping for bridges in air that may significantly alter the dynamics when feedback is present. This is evident from the lumped-parameter model indicating that the delay τ must be sufficiently short (Marr-Lyon *et al.* 1997). For long bridges, from physical considerations, the magnitude of the boundary-layer coefficient in the characteristic equation for the complex natural frequency of the mode is strongly influenced by the presence of a liquid outer bath. The model suggests that the influence of delayed feedback on mode stability may be different for bridges in air than for bridges in Plateau tanks. It is plausible that τ may need to be significantly smaller for bridges in air than for bridges in Plateau tanks. Consequently even with the prior success of active stabilization of long bridges in Plateau tanks (Marr-Lyon *et al.* 2000) it was not certain that $\tau \approx 0.03\,\mathrm{ms}$ was sufficiently small to facilitate the stabilization of long bridges in air for the bridge viscosity considered.

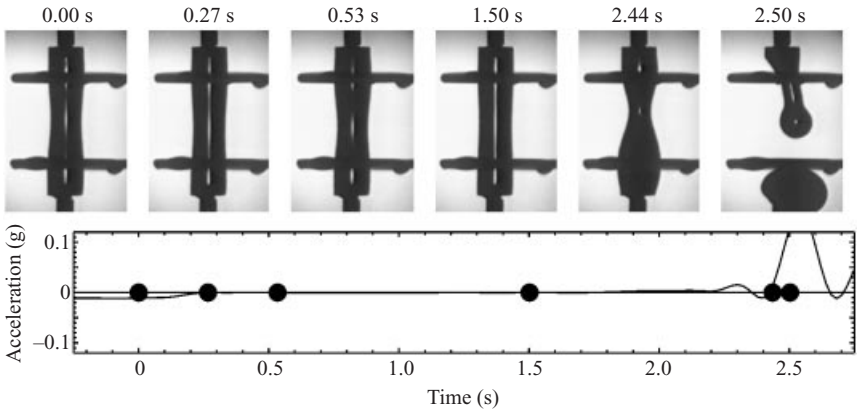

FIGURE 3. Liquid bridge stabilized to a slenderness of 3.6 by the bias-potential method. The bridge broke due to the disturbance shown in the accelerometer trace starting at around 2.4 s. Here and in subsequent figures the displayed portion is near the end of the low-gravity interval with $t = 0$ being shortly after bridge extension was complete.

4. Results

4.1. *Stabilization*

Both the bias-potential and square-root methods have been successfully tested on the KC-135. Initial observations clearly indicated that it was possible to extend the slenderness significantly beyond π. Turning off the control after several seconds of stabilization shows that the bridge breaks in much less than one second from the growth of the (2,0) mode as previously shown with acoustic stabilization (Marr-Lyon *et al.* 2001). The results discussed below were obtained after the sensitivity of the control system was improved and under excellent flying conditions. Several deployment records support the conclusion that the growth of the (2,0) mode may be suppressed. Results are presented as time-sequence images with the associated accelerometer trace beneath. The dots on the accelerometer trace correspond to the times at which the images were taken. Figure 3 shows the result of stabilization using the bias-potential method. The bridge liquid in this case was an aqueous solution of 63.9 wt% glycerol and 9.0 wt% NaCl (viscosity ∼ 25 cS). The bridge was stabilized to a slenderness of 3.6 for several seconds before breakage occurred due to a disturbance in the acceleration level. The volume was determined by digital image analysis to be constant prior to breaking. The normalized bridge volume, $V/\pi R^2 L$, in this case was 0.965 and the bias-potential was 450 V. During the quiescent period, the bridge has a static (3,0)-mode shape with bulges near each end and a small diameter in middle. This is because the volume of the bridge is below that of a circular cylinder and is enhanced because of the bias potentials on the ring electrodes. Such shapes have also been observed in Plateau-tank experiments (Marr-Lyon *et al.* 2000).

The longest bridges on the KC-135 have been achieved using the square-root algorithm. The results presented here will be discussed in the context of the stability diagram shown in figure 6 which was computed following the methods of Lowry & Steen (1995) for a bridge in zero gravity. The stability diagram for this part of parameter space has been presented by Lowry (2000) and Marr-Lyon *et al.* (2000). The equilibrium shapes shown in the shaded regions of figure 6 are unstable to the (2,0) mode. The white regions of the plot are unstable to both the (2,0) and (3,0) modes and thus could not be stabilized with the current two-electrode array. The

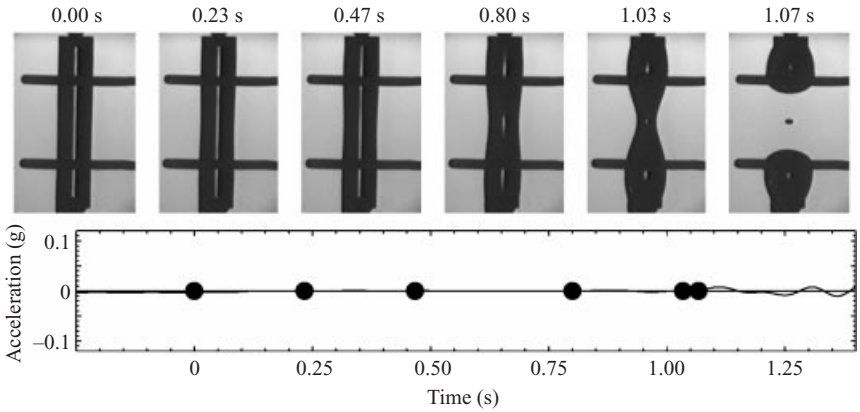

FIGURE 4. Active control using the square-root feedback algorithm suppressed the growth of the (2,0) mode for a bridge in air. This bridge has $S = 4.3$ and is observed here under the very best of circumstances. Break-up in this example is apparently from the natural growth of the (3,0) mode because of the observed symmetry.

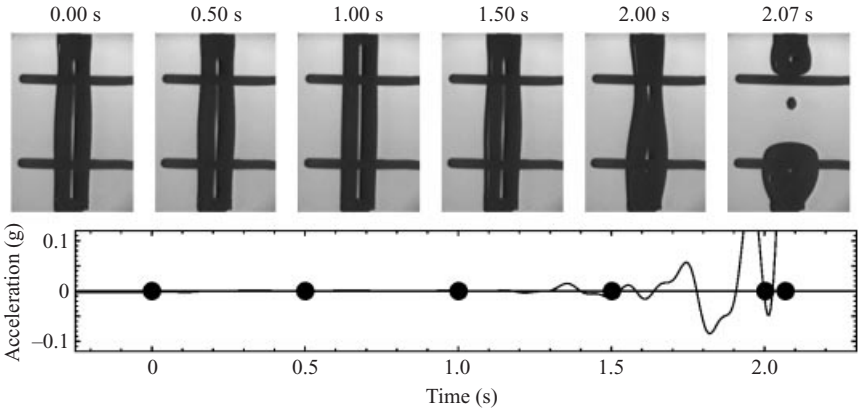

FIGURE 5. Stabilized bridge of slenderness 4.4 using active control with the square-root algorithm.

shaded regions of the plot thus show conditions for which the square-root stabilization method should work. The stability boundaries for the bias-potential method would be expected to be shifted since the bias potentials on the electrodes modifiy the equilbrium shape of the bridge. Figure 4 shows a bridge stabilized at a slenderness of 4.3 for about 1 s before disturbances cause the bridge to break in the (3,0)-mode configuration. The bridge liquid was an aqueous solution of 43.5 wt% glycerol and 1.0 wt% NaCl (viscosity $\sim$ 4 cS). The normalized volume determined from image analysis is 0.993. This bridge was very close to the lower stability boundary as shown in figure 6, thus only a small disturbance is necessary to cause bridge breakage from the growth of the (3,0) mode. A result from a different parabola on the same day, with the same liquid, is shown in figure 5 for a slenderness of 4.4 and normalized volume of 1.026. Although this bridge is longer it is not as near to the stability boundary since it is 2.6% higher in volume (see figure 6). This bridge survived a significant disturbance, seen in the accelerometer record, before finally rupturing in response to an even larger disturbance. The bridge appeared to break from the growth of the (2,0) mode.

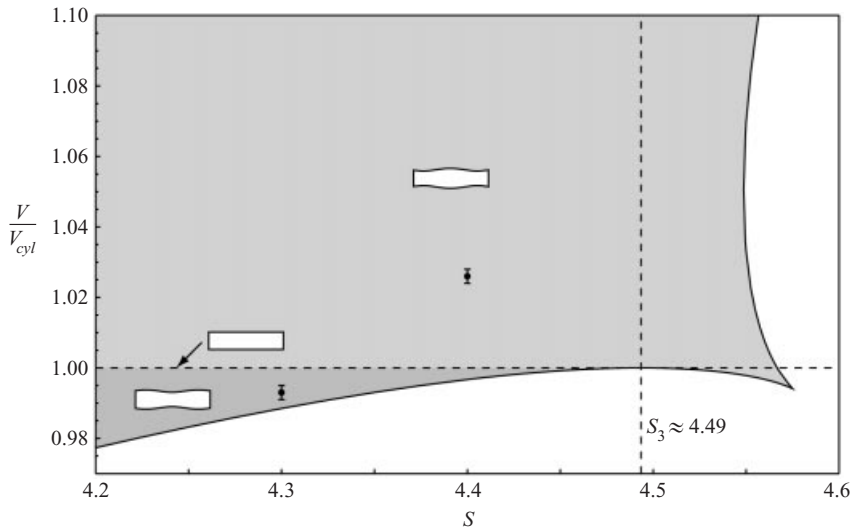

FIGURE 6. Stability boundaries near the upper slenderness limit for stabilization by the two-electrode method. The shaded regions are normally unstable to (2,0)-mode perturbations and the white regions are unstable to both (2,0)- and (3,0)-mode perturbations. The (unstable) equilibrium shapes are shown for the different domains. The two data points correspond to the two longest bridges stabilized to date (the bridges shown in figures 4 and 5). The error bars indicate the uncertainty in the bridge volume from digital image analysis. The mean and standard deviation are shown from over 30 images of each bridge.

4.2. *Oscillation and free decay*

In addition to stabilization experiments, bridge oscillations were recorded. Information can be obtained either by purposely exciting the (2,0) mode oscillation by modulating the electrode potentials or by observing the dynamics of the bridge following an accidental bump to the apparatus which sometimes excites the (2,0) mode and other modes. Modulation of electrode potentials can be used to drive the (2,0) mode exclusively in order to measure the natural frequency and damping of the mode. A burst of modulation is used to excite the mode while the mode amplitude is monitored as shown in figure 7. The results in figure 7 are for a 3.7 cS bridge of slenderness 2.4 without feedback. The frequency and decay time ($1/e$) of the (2,0) mode measured from the data in figure 7 were 4.9 Hz and 0.92 s respectively. The measured density and surface tension for the bridge liquid were 1.115 g cm^{-3} and 64.4 dyn cm^{-1} respectively. For these values of the bridge properties and a bridge radius of 0.216 cm, a semi-analytical, linear theory of cylindrical bridge oscillations by Nicolás & Vega 2000 predicts a frequency of 5.2 Hz and a decay time of 1.4 s. The inviscid theory of Sanz & Diez (1989) also predicts a frequency of 5.2 Hz for these conditions. The volume of the bridge measured from image analysis was 1.3% below the assumed cylindrical value. In Plateau-tank experiments, a volume deficiency of 1% was found to decrease the frequency by 3% which is in the same direction. Uncertainties in the properties owing to an uncertainty in the liquid temperature during the flight may also contribute to disagreement between theory and measurement. Decay times increase for longer bridges making accurate measurements difficult in the limited duration of low gravity available on the KC-135.

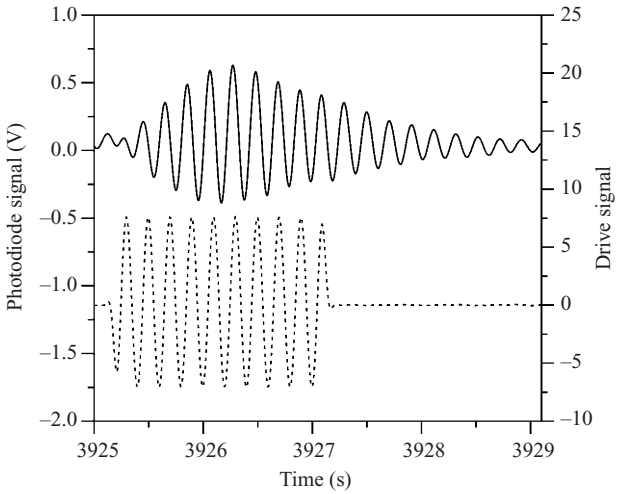

FIGURE 7. The driven oscillation and decay of the (2,0) mode of a bridge with slenderness 2.4. The solid curve is the photodetector signal which is proportional to the (2,0) mode amplitude while the dashed curve is the drive signal sent to the feedback circuit to modulate the electrode potentials. The drive frequency differs from the natural frequency since the latter was not known prior to the measurement.

5. Discussion and summary

Observations of the kind shown in figure 4 giving symmetric breakup associated with the growth of the (3,0) mode are extremely rare. Figure 4 shows the best event observed in a large number of trials. It appears likely that such observations require not only that the effective gravity and g-jitter is small during the final stages of the observation but also that high-quality low gravity is maintained for about 10 s while the bridge is initially extended. That is because of the long decay time for vibrations accidentally introduced on long bridges. Significantly raising the viscosity of the bridge causes the viscous stresses during the rapid deployment of the bridge to increase and slows down the breakup once the stability boundary is reached. Consequently it may be impractical if not impossible to probe the predicted (3,0) mode stability boundary, figure 6, using bridges in air on the KC-135 though it is plausible that this could be done on a space-based platform.

This research was supported by the National Aeronautics and Space Administration.

REFERENCES

BURCHAM, C. L. & SAVILLE, D. A. 2000 The electrohydrodynamic stability of a liquid bridge: microgravity experiments on a bridge suspended in a dielectric gas. *J. Fluid Mech.* **405**, 37–56.

CASTELLANOS, A. & GONZÁLEZ, H. 1994 Stability of inviscid conducting liquid columns subjected to a.c. axial magnetic fields. *J. Fluid Mech.* **265**, 245–263.

CHEN, Y. J., ROBINSON, N. D., HERNDON, J. M. & STEEN, P. H. 1999 Liquid bridge stabilization: theory guides a codimension-two experiment. *Comput. Meth. Appl. Mech. Engng* **170**, 209–221.

COCKAYNE, B. 1968 Developments in melt-grown oxide crystals. *J. Cryst. Growth* **3**, 60–70.

LIN, S. P. & REITZ, R. D. 1998 Drop and spray formation from a liquid jet. *Annu. Rev. Fluid Mech.* **30**, 85–105.

LOWRY, B. J. 2000 The double-helical branch structure of fixed contact line liquid bridge equilibria. *Phys. Fluids* **12**, 996–1004.

Lowry, B. J. & Steen, P. H. 1995 Capillary surfaces: stability from families of equilibria with application to the liquid bridge. *Proc. R. Soc. Lond.* A **449**, 411–439.

Lowry, B. J. & Steen, P. H. 1997 Stability of slender liquid bridges subjected to axial flows. *J. Fluid Mech.* **330**, 189–213.

Mahajan, M. P., Tsige, M., Zhang, S., Alexander, J. I. D., Taylor, P. L. & Rosenblatt, C. 2000 Collapse dynamics of liquid bridges investigated by time-varying magnetic levitation. *Phys. Rev. Lett.* **84**, 338–341.

Marr-Lyon, M. J., Thiessen, D. B., Blonigen, F. J. & Marston, P. L. 2000 Stabilization of electrically conducting capillary bridges using feedback control of radial electrostatic stresses and the shapes of extended bridges. *Phys. Fluids* **12**, 986–995.

Marr-Lyon, M. J., Thiessen, D. B. & Marston, P. L. 1997 Stabilization of a cylindrical capillary bridge far beyond the Rayleigh–Plateau limit using acoustic radiation pressure and active feedback. *J. Fluid Mech.* **351**, 345–357.

Marr-Lyon, M. J., Thiessen, D. B. & Marston, P. L. 2001 Passive stabilization of capillary bridges in air with acoustic radiation pressure. *Phys. Rev. Lett.* **86**, 2293–2295; and erratum **87** (20), 9001.

Nahas, N. M. & Panton, R. L. 1990 Control of surface-tension flows: instability of a liquid jet. *Trans. ASME*: *J. Fluids Engng* **112**, 296–301.

Nicolás, J. A. & Vega, J. M. 2000 Linear oscillations of axisymmetric viscous liquid bridges. *Z. Angew. Math. Phys.* **51**, 701–731.

Powers, T. R., Zhang, D., Goldstein, R. E. & Stone, H. A. 1998 Propagation of a topological transition: the Rayleigh instability. *Phys. Fluids* **10**, 1052–1057.

Ramos, A., Gonzalez, H. & Castellanos, A. 1994 Experiments on dielectric liquid bridges subjected to axial electric fields. *Phys. Fluids* **6**, 3206–3208.

Rao, M. M. & Shyy, W. 1997 Moving boundary computation of the float-zone process. *Intl J. Numer. Meth. Engng* **40**, 1231–1261.

Sankaran, S. & Saville, D. A. 1993 Experiments on the stability of a liquid bridge in an axial electric field. *Phys. Fluids* A **5**, 1081–1083.

Sanz, A. & Diez, J. L. 1989 Non-axisymmetric oscillations of liquid bridges. *J. Fluid Mech.* **205**, 503–521.

Schatz, M. F. & Neitzel, G. P. 2001 Experiments on thermocapillary instabilities. *Annu. Rev. Fluid Mech.* **33**, 93–127.

Sumner, L. B. S., Neitzel, G. P. Fontaine, J. P. & Dell'Aversana, P. 2001 Oscillatory thermocapillary convection in liquid bridges with highly deformed free surfaces: Experiments and energy-stability analysis. *Phys. Fluids* **13**, 107–120.

Velten, R., Schwabe, D. & Scharmann, A. 1991 The periodic instability of thermocapillary convection in cylindrical liquid bridges. *Phys. Fluids* A **3**, 267–279.